Closed-loop control of hydraulic telescopic handler

Justin Činkelj*, Roman Kamnik, Peter Čepon, Matjaž Mihelj, Marko Munih

Laboratory of Robotics and Biomedical Engineering, Faculty of Electrical Engineering, University of Ljubljana, Tržaška cesta 25, 1000 Ljubljana, Slovenia

Abstract

Automatization is supposed to improve working conditions and safety in construction industry, as it already did in manufacturing industries. This paper presents the development of a robotic control system for a commercially available hydraulic telescopic handler. The target application for the telescopic handler is semi-automated assembly of facade panels. The base handler was upgraded with two additional hydraulic axes, position sensors and closed-loop control system, while the original handler safety assurance mechanisms were preserved. The control approach is based on a PI controller with velocity feedforward and valve overlap compensation. The direct and inverse kinematic models of handler mechanism were developed to enable control of end-effector motion along a straight line in Cartesian coordinate system. The motion performances were evaluated following the ISO 9283 standard with payload of 2000 kg. Results show the repeatability of positioning bellow 7.0 mm and the straight line tracking error smaller than 63 mm.

Key words: hydraulic telescopic handler, robot, closed-loop control

1. Introduction

Construction industry is one of the most important industry sectors worldwide. It contributes a large part of gross domestic product and offers jobs to many workers [1]. Many work tasks are still performed manually. This is in contrast with other industries, where automated machines and robots became indispensable. Automation is considered not only as beneficial, but as required [2]. Also the working conditions are uncomfortable compared with manufacturing industries [3].

It is usually difficult to directly transfer solutions from a factory floor to a construction site. The working environment is typically unstructured and changing with full richness of a natural setting. Required infrastructure for automation (for example, to enable localization of items) is not available. Installation of such infrastructure would be difficult, if not impossible [4].

One approach for solving the problem associated with unstructured environment is "conversion" of construction site into a factory [5]. Protective roof improves working conditions for workers and increases labor productivity. Another successful application of an automated building system is presented in [6]. Applied solution was proven to be no more expensive than the use of a tower crane and the building time was within schedule.

These examples of automation are among the most automated solutions. Technologies like automated delivery system have to be available or developed [7]. Whole construction process has to be compatible with automation. Thus, such solutions cannot be applied for renovation of older buildings. It can be difficult to reuse the technology even in a case of new buildings, due to construction projects that are usually one-off and unique [8]. The automated building system in [6] was successful, yet still applied only once. To reduce compatibility problem between traditional and automated workflow often only a single machine, or even a single machine operation is automated.

Hydraulic machines (excavators, dumpers, cranes and handlers) are widely used in construction due to ruggedness and high power to mass ratio. They are exclusively operated manually, via a joystick or with a radio remote control. Manually controlled

*Corresponding author. Tel.: +386 1 4768-191, fax: +386 1 4768-239

Email address: justin.cinkelj@robo.fe.uni-lj.si (Justin Činkelj)

commercial devices cannot assure straight line motion of excavator bucket or handler end-effector. Computer control can improve motion performance of a hydraulic device in this respect.

In [9] authors focus on a problem of telescopic handler end-effector vibrations. Solution is based on the use of a computer generated reference trajectory, which avoids vibrations by not exciting natural frequency of the handler telescope. In [10] a teleoperation system for a mini excavator is presented. The operator was able to move the bucket along a straight line, with performance comparable to the standard control via joystick. Another mini excavator was automated with a goal to ease straight line movement [11]. Authors explicitly avoided using sensors for position feedback. Instead, they relied on load-independent feature of Sauer-Danfoss PVG 32 valves. Linear motion experiment with velocity of 2 m/min in homogenous soil resulted in position deviation of about 4 cm for movement length of 110 cm. An autonomous robotic excavator is presented in [12]. Ability to deal with obstacles along the trench line was necessary for real-world application. Production rule based artificial intelligence system chose suitable strategy, first for removing the soil around the obstacle, and then to dig the obstacle. Laying of buried pipes is dangerous due to the wall caving. Developed tele-robotic system with a special gripper device enabled pipe laying and joining with no workers below surface [13]. Two hydraulic robots for robotized masonry were developed in ROCCO project [14]. The larger machine has a reach of 8.5 m and payload of 500 kg. Controller utilized a gain scheduling scheme, where gains were adjusted by a fuzzy supervisory system. The RoboTab-2000 robot from [15, 16] was a tool for installation of 70 kg heavy plaster panels for indoor wall. The 6 degrees of freedom (DOFs) robot was closed-loop controlled with two joysticks, one dedicated for position and the second for orientation of the robot end-effector. This user interface was proven to be easy to learn and intuitive even for inexperienced operator. In [17] a 6 DOFs hydraulic robot named Starlifter was presented. A case study for drilling holes into motorway bridge proposed mounting the robot on a telescopic crane increasing the workspace. Applications of large scale manipulators included automated washing of airplanes [18]. Benefits were obtained due to shortened ground time (three to four times compared to manual cleaning), lower fuel consumption and extended paint life.

In the present paper, the development of a large scale 6 DOFs robotic manipulator is presented. The development is based on a commercially available telescopic handler. The robotized manipulator is aimed to be part of a system for semi-automated construction of montage buildings. In particular, it is aimed at placing and fixing facade panels to the facade.

Panels, made of two metal sheets with mineral wool in between, are 1 m wide, up to 12 m long and weight up to 500 kg. The existing manual approach for montage facade assembly utilizes hydraulic telescopic handler and two groups of workers. First group of workers prepares the panel and attaches it to a steel wire, suspended from the telescopic handler. Handler operator moves the panel in vicinity of the facade, where the second group manually aligns the panel with facade and fixes it. Two main tasks are identified: a) panel transport from the palette to the facade, and b) fixation of the panel to the facade.

The designed semi-automated assembly system consists of two main parts. The first part is a 6 DOFs hydraulic telescopic handler, used as a macromanipulator for gross movement of panels from the palette to the facade. At the handler end-effector a micromanipulator is mounted, performing final alignment of the panel with the facade and fixing the panel to the steel beams.

For the semi-automatic panel assembly, the handler should be able to operate with high degree of autonomy. Thus, the handler has to be able to manipulate facade elements without operator involvement. Main functional requirements are 6 active DOFs, synchronized multi-axis motion and programmed point-to-point motion in Cartesian coordinate system. The required positional accuracy is better than 10 cm. Expected payload at the handler end-effector including facade panel, micromanipulator, vacuum grippers, drilling and fixation systems is 2000 kg. Such machine is not readily available on the market.

The closed-loop control system for commercial telescopic handler meeting the above requirements is presented in this paper. The original handler and required upgrade of its mechanics, hydraulics and sensor feedback are introduced in section 2. Control system hardware and closed-loop control algorithms are presented in section 3. Procedures for evaluation of motion performance are explained in section 4. Results of evaluation are outlined in section 5, followed by conclusions in section 7.

2. Base system

A hydraulic telescopic handler with maximum payload of 4500 kg and maximum forward reach of 18 m was purchased as a base system. Hydraulic subsystem is built around directional spool valves and a load-sensing hydraulic pump.

Load-sensing pump operates with variable flow and pressure, both being controlled by load pressure. Typical property of load-sensing system is its relatively slow response compared to a system with constant system pressure. The pump increases its output flow/pressure in response to increased load pressure, what causes delayed response. Tests on machine showed that after step change of valve control voltage time required to reach 90% of velocity change is typically about 0.5 s, and can be much larger if operating at low velocities.

Used hydraulic valves are originally intended for manually operated machines. This implies that valve spool has a large overlap to prevent oil leakage when the valve is closed. Spool overlap introduces deadband into valve input-output characteristics, which is problematic for closed-loop control due to imposed nonlinearity.

The machine stability on ground is originally monitored by a dedicated overload detection unit, measuring load on all four stabilizers to detect overturn conditions. In the vicinity of overturn conditions, the overturn event is prevented by turning off the hydraulic power supply to the six directional spool valves by closing the main valve. As a last safety assurance, unintended handler telescope motion can be stopped by pressing the emergency stop push button. This action shuts down the diesel engine driving the hydraulic pump. One of the main requirements of controller upgrade was to preserve the original manual operation mode of the handler, and all existing safety subsystems fully functional all the time.

2.1. Modification of handler mechanics

In original configuration, the machine had 4 independent DOFs (axis 1: turret rotation, axis 2: telescope lift, axis 3: telescope extension and axis 4: fork tilt). To enable arbitrary position and orientation of the handler end-effector, two additional joints were added at the end of the telescope. Fig. 1 presents handler with modified mechanics (axis 5: yaw (left-right) rotation, axis 6: roll rotation).

In Fig. 2 a hydraulic circuit for driving all 6 axes is shown. The 2^{nd} (telescope lift) and 4^{th} (fork tilt) axes are connected by additional compensating hydraulic parallelogram circuit. This way, motion of 2^{nd} axis drive the compensating cylinder (labelled in Fig. 2 as *Comp*). Oil flow from the compensating cylinder flows to the 4^{th} cylinder via a summing valve (labelled as $\sum$). This ensures that handler forks remain horizontal during telescope lift without controlling the 4^{th} axis. The 5^{th} axis utilizes hydraulic cylinder. The 6^{th} axis consists of a hydraulic motor and a spindle driving a gear wheel. Resolution of position measurement for each axis is given later in Table 2.

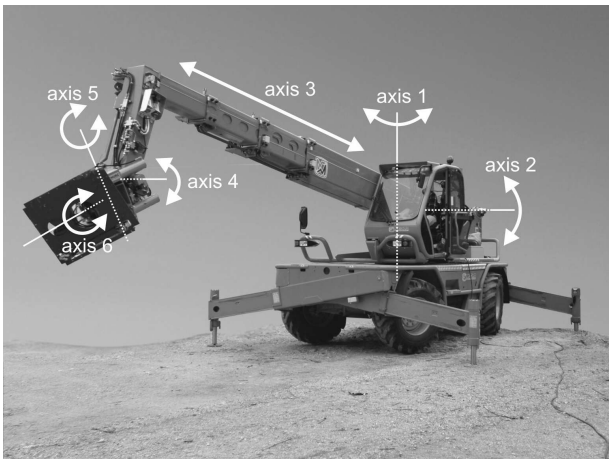

Figure 1: The telescopic handler with two additional axes. Axes motion directions are marked by arrows.

2.2. Position sensors implementation

For a closed-loop control of the handler end-effector a position feedback is required. For this purpose a set of position sensors is implemented on handler's axes. Telescope length is measured by a wire draw sensor, while rotation angles are measured by resolvers. The sensors are interfaced via CAN bus.

The telescope mechanics consists of four segments driven by a hydraulic cylinder and chain pulley. The telescope length sensor measures distance between the 1^{st} and the 4^{th} (last) telescope segment. This configuration eliminates error due to chain looseness.

Resolvers for the 2^{nd}, 4^{th} and 5^{th} axis are installed directly on rotational axes. Such installation is not possible for the 1^{st} and 6^{th} axes, because they are realized with a large internal gear wheel with a hole in its center. Thus, the 6^{th} axis sensor is attached on the hydraulic motor driving the axis. The

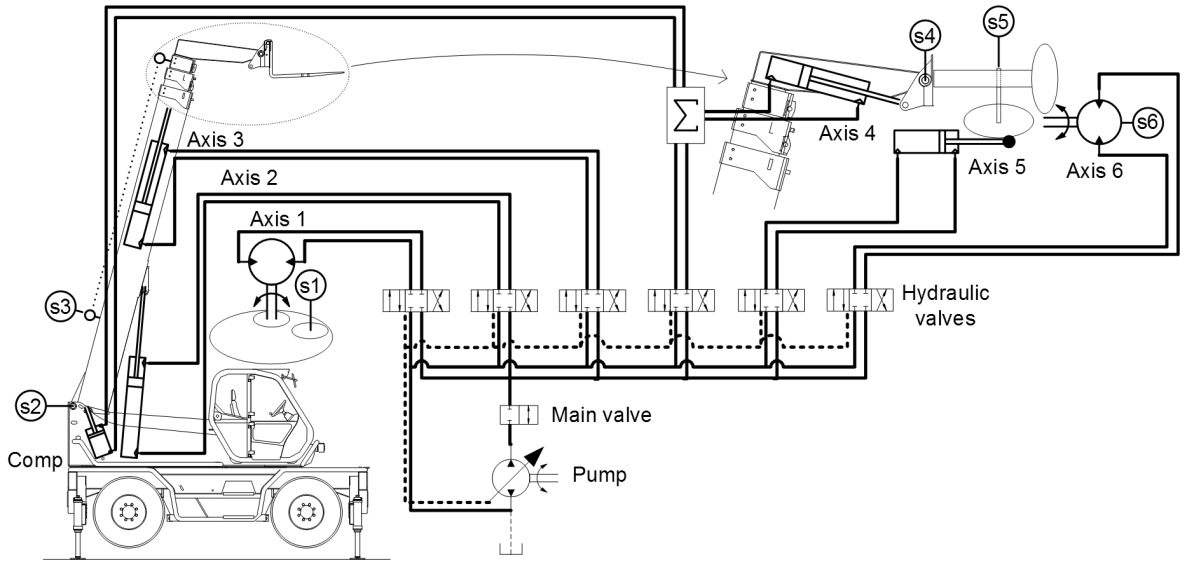

Figure 2: Simplified hydraulic circuit of hydraulic telescopic handler. Main components are pump, hydraulic valves and actuators. Bold solid lines indicate main pipes from the pump to the valves and actuators. Dashed lines indicate load-sensing pipes from valves to the pump. Compensation cylinder and summing valve for the 4^{th} axis are labelled as *Comp* and $\sum$. Position sensors are marked as $s1$ to $s6$.

1^{st} axis sensor measures turret rotation by an additional measuring gear geared with the large internal gear wheel. The measuring gear is made of two gears, connected by a pre-tensioned torsion spring to eliminate backlash between the measuring gear and the gear wheel.

3. Development of a 6 DOFs robotic control system

3.1. Control system hardware

In Fig. 3, the original handler subsystems are shown in the lower half, below the dashed line. In the upper half, above the dashed line, the additional hardware components required for robotic control are shown. A selector switch for selecting original or closed-loop operation mode was added to the operator control board.

Two PC-based computers are used for closed-loop control of the telescopic handler. The first is a graphical user interface (GUI) PC with a touch screen monitor, used for interaction with the operator and communication with higher-level system. In Fig. 4 an operator workspace inside handler's cab is shown. Part of the GUI application with movement buttons on the screen is used for jogging movement of the handler. Three different coordinate systems are available (joint, world and tool). Jogging step is individually selected for each axis. As an alternative, the operator can use two three-axial joysticks for manually directing handler along a straight line in selected coordinate system.

The second PC is the real-time (RT) controller for control of handler motion in hard real-time. The RT controller output is the control voltage for hydraulic valves. In the closed-loop mode of operation, the joystick is used as an option for manually directing handler motion along a straight line in Cartesian space.

The valve control voltages from both RT and original controller are feed to the watchdog timer (WDT) module. The WDT module switches between both signal sources based on a signal from the original/closed-loop mode selector switch. Additional task for the WDT module is monitoring a real-time performance of the RT controller. The WDT module would stop the motion in the case the RT controller would fail to satisfy real-time constraints.

3.2. Servo valve identification

The servo valve main characteristic is presented by control voltage to oil flow diagram. The characteristic was recorded for all six axes on a telescopic handler. It was assessed by applying a constant control voltage and measuring velocity of the corresponding actuator. The oil flow was computed

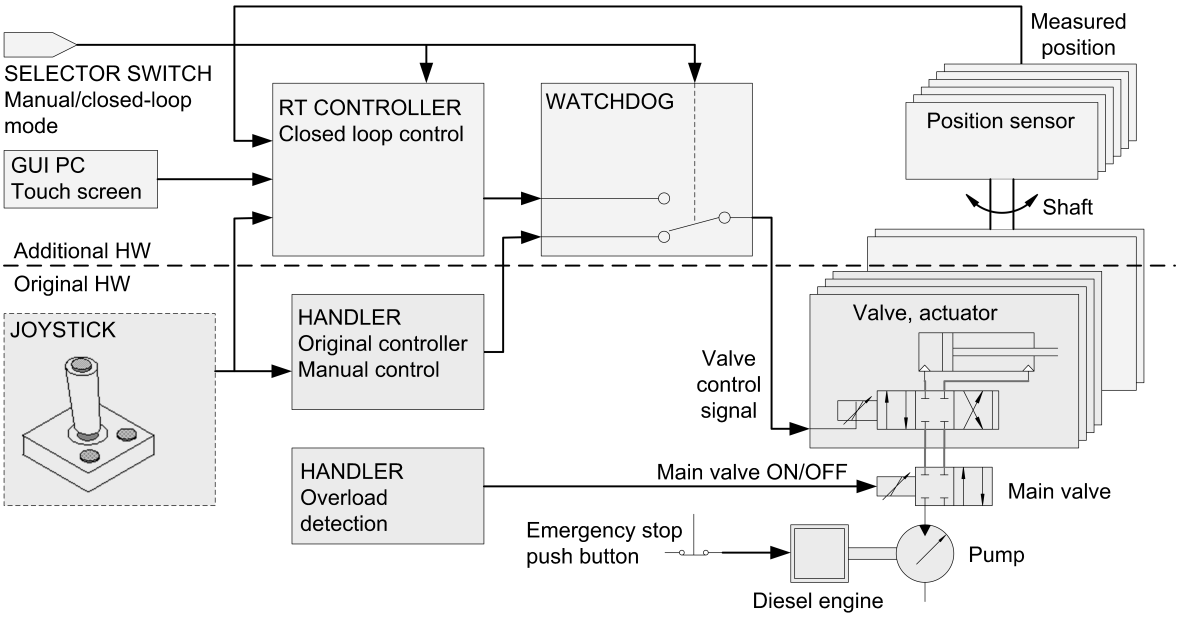

Figure 3: Hardware components of the closed-loop controlled handler. Below the dashed line: controller components of the original handler. Above the dashed line: additional controller components of the closed-loop control.

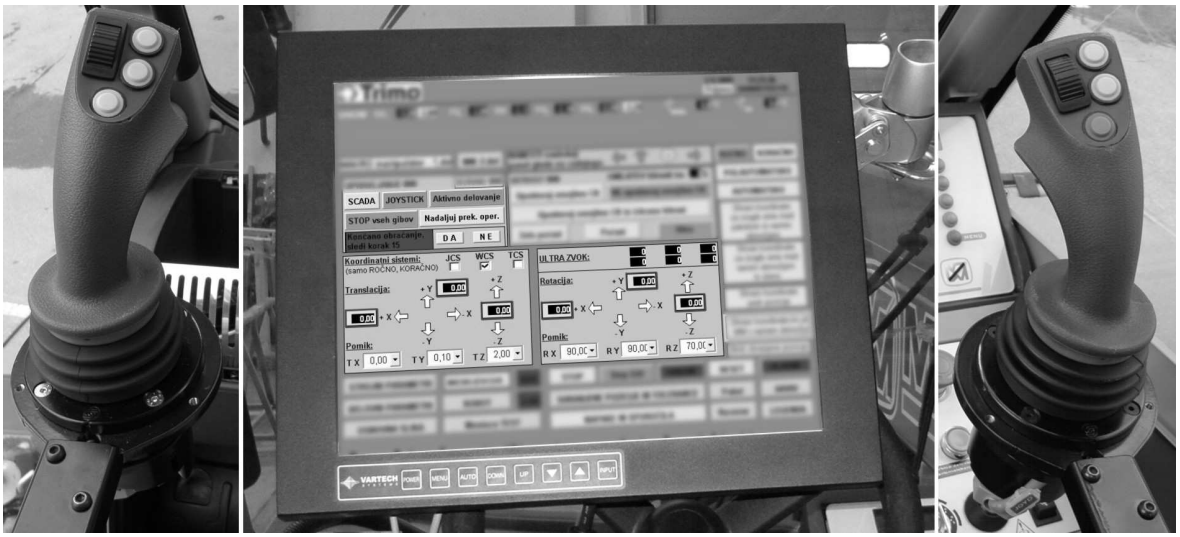

Figure 4: Operator workspace inside handler's cab. With the GUI application (on the screen in the middle) operator first selects jogging step for desired axis and than triggers motion by pressing appropriate arrow. As an alternative, two three-axial joysticks can be used for manually directing handler along a straight line.

based on the actuator velocity and known cylinder geometry (or hydraulic motor volume). On Fig. 5 two examples for the telescope lift and extension axes valves characteristics are shown. The valve overlap around 2.5 V control voltage is evident. The threshold values, required to start motion in negative/positive direction, are denoted as U_{th_m}/U_{th_p}, respectively.

3.3. Closed-loop control

Control software for closed-loop control is running on the RT controller. The software is implemented in Matlab/Simulink/xPC Target environment. The Matlab/Simulink environment offers

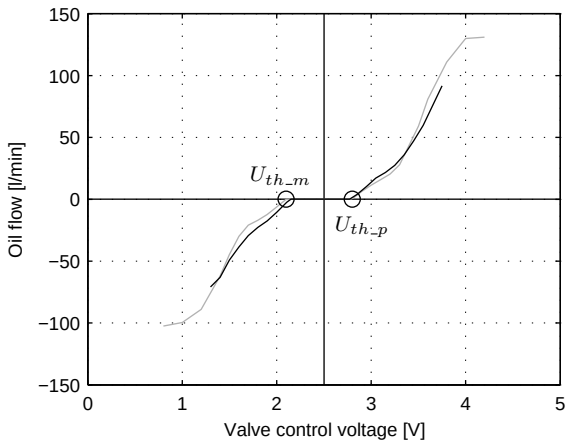

Figure 5: Measured oil flow vs. signal voltage characteristics of the telescope lift (black curve) and telescope extension (gray curve) axes. Overlap around 2.5 V (valve offset voltage) is evident.

user friendly software development environment, graphical programming mode and powerful support for matrix calculation and numerical methods. The xPC Target is used for deployment and execution of developed algorithms in real-time operating system.

The end-effector motion is controlled by six individual controllers operating in joint space. Each joint space controller generates valve control voltage in a closed loop to assure that measured joint position tracks the reference value. A proportional-integral (PI) controller with overlap compensation and velocity feedforward was chosen for control. Sampling frequency is 100 Hz. The controller is described by equation (1) and graphically depicted in Fig. 6. Symbol $\dot{q}_r$ stands for the reference velocity, while symbol q_e for positional error, i.e. difference between the reference position q_r and measured position q_m.

$$
\begin{aligned}
U_{act\_tmp} &= K_{vf}\dot{q}_r + K_p q_e + K_i \int q_e dt \qquad (1)\\
U_{act} &= \begin{cases} U_{th\_m} + U_{act\_tmp}, & U_{act\_tmp} < 0 \\ 0, & U_{act\_tmp} = 0 \\ U_{th\_p} + U_{act\_tmp}, & U_{act\_tmp} > 0 \end{cases}\\
U_{th\_m} &= (2.5 - cca.\ 0.3)\ V\\
U_{th\_p} &= (2.5 + cca.\ 0.3)\ V
\end{aligned}
$$

The velocity feedforward (gain K_{vf}) is introduced to improve tracking and speed up the system response. The proportional gain contribution

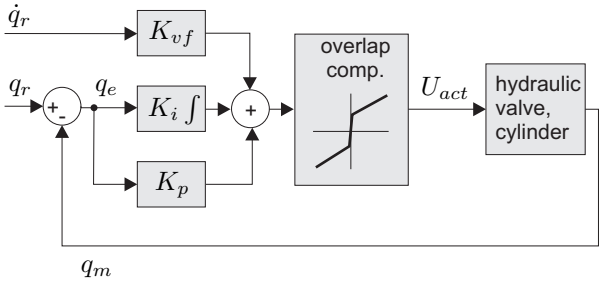

Figure 6: Structure of the implemented closed-loop controller for a single hydraulic axis

(parameter K_p) reduces positional error. The integral part (parameter K_i) reduces steady state positional error. The overlap compensation eliminates deadband caused by the spool overlap by adding additional offset voltage (U_{th_m} or U_{th_p}).

For controllers that control asymmetrical linear actuators two sets of gains are defined, one for positive and one for negative motion direction. In case of linear actuators the position control is performed at the level of actuator displacement, meaning that reference/measured position and velocity (q, $\dot{q}$) in equation (1) refer to cylinder displacement/velocity (L, $\dot{L}$) instead of joint position/velocity (θ, $\dot{\theta}$).

The initial controller gain values were determined by means of simulation. The gain values were fine-tuned later on the real handler. Reference trajectories used for fine-tuning included sinusoidal and trapezoid velocity profiles.

A simulation model of axes motion was identified from measured open loop responses to a set of step excitations. The axis response for each single step excitation was modelled as a local linear model. Local models were then merged into a nonlinear model by applying a local model network technique [19, 20].

3.4. Kinematic model

3.4.1. Joint to WCS transformation

To enable straight line interpolated motion in Cartesian world coordinate system (WCS) a kinematic model was developed. Forward kinematic model is used for calculating position and orientation of the handler end-effector in WCS on the basis of measured joint positions. The handler has a serial kinematic chain configuration with a RRTRRR structure (R - rotational axis, T - translational axis, first letter describes first axis etc.). Kinematic model is described with the Denavit-Hartenberg (D-H) notation [21]. The D-H notation

systematically expresses pose of each mechanism's segment relative to the previous segment with a set of four parameters. The handler's D-H parameters are listed in Table 1.

For closed-loop control during point-to-point move in WCS, all points between the start and stop point have to be determined via trajectory interpolation. A trapezoid velocity profile is used for trajectory interpolation. Each pose coordinates are transformed from WCS to joint axis positions via inverse kinematics. As the analytical solution of inverse kinematic model does not exist for the particular mechanism[1] an iterative numeric algorithm is applied according to [22]. The algorithm is based on WCS to joint coordinate system (JCS) velocity transformation made with analytical Jacobian matrix J. WCS velocity is obtained by multiplying Jacobian matrix and JCS velocity.

The general principle of the basic algorithm for obtaining the inverse kinematic solution is described by equation (2) (for robust realization, which prevents drift of obtained joint position due to numerical integration, please see [22]). Current iteration step is marked with t_k. Based on the reference velocity ($v(t_k)$) expressed in WCS and known current position expressed in JCS ($q(t_k)$) the needed JCS pose change ($\Delta q(t_k)$) is determined. New position of joints is then determined by adding $\Delta q(t_k)$ to the current joint position.

$$\begin{aligned} \Delta q(t_k) &= J^{-1}(q(t_k))v(t_k)\Delta t \\ q(t_{k+1}) &= q(t_k) + \Delta q(t_k) \end{aligned} \tag{2}$$

The algorithm requires computation of the inverse Jacobian matrix J^{-1} in each iteration step. The existence of the inverse is not guarantied (it does not exists in singular poses). Singular poses originate from the kinematic structure (determinated by mechanical configuration) or from the selected mathematical representation of the end-effector orientation. The end-effector orientation representation was selected such that singularities occur outside of the useful workspace.

Numerical value of the Jacobian matrix J is obtained from geometric Jacobian matrix J_g. The J_g is derived via iterative procedure described in [22], requiring Denavit-Hartenberg parameters and current joint positions as an input.

[1] Analytical solution to inverse kinematics problem exists if three consecutive revolute axes intersect at a common point or are parallel [22].

3.4.2. Actuator to joint transformation

As noted in section 3.3, for the axes driven by linear hydraulic actuators the closed-loop control is performed at the level of cylinder length. The relationship between cylinder length and axis angle is nonlinear for the telescope lift and fork tilt axes. The compensation cylinder length is also incorporated in the nonlinear relationship. The mechanical arrangement of all three cylinders is shown on Fig. 7 and Fig. 8.

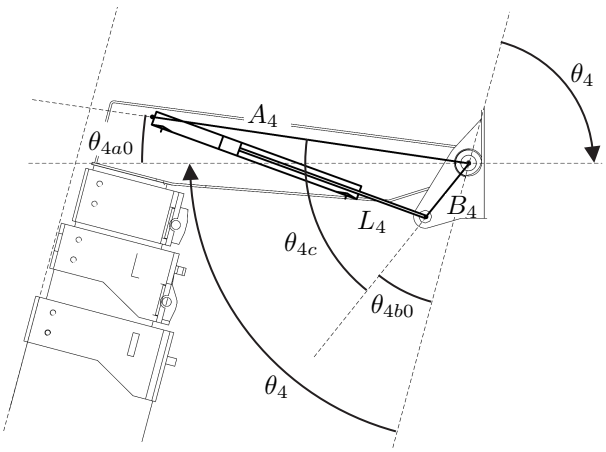

Figure 8: Nonlinear transformations between axis angular position and cylinder length for the 4^{th} axis

The telescope lift cylinder length is marked with L_2, and forms triangle with A_2 (distance from axis center of rotation to the fixed end of cylinder) and B_2 (distance from axis center of rotation to the moving end of cylinder). Variable θ_{2c} denotes the angle between A_2 and B_2. Telescope lift axis angle θ_2 is measured from the horizontal level. Angles θ_{2a0} and θ_{2b0} are constants. Cylinder length L_2 and velocity $\dot{L_2}$ are expressed as a function of angle θ_2 according to cosine law (3).

$$\begin{aligned} \theta_{2c} &= \theta_2 + \theta_{2a0} - \theta_{2b0} \\ L_2 &= \sqrt{A_2^2 + B_2^2 - 2A_2B_2cos(\theta_{2c})} \\ \dot{L_2} &= \frac{A_2B_2sin(\theta_{2c})}{L_2}\dot{\theta_2} \end{aligned} \tag{3}$$

Transformations for the fork tilt axis are described in (4), and for the compensation cylinder in (5). Symbols are named as for the 2^{nd} (telescope lift) axis, only that subscript $_4$ denotes the 4^{th} (fork tilt) axis and subscript $_c$ the compensation cylinder.

Table 1: Set of Denavit-Hartenberg parameters describing kinematic model of telescopic handler.

Axis number	Axis description	a $[m]$	α $[rad]$	d $[m]$	θ $[rad]$
1	Turret rotation	-2.400	$+\pi/2$	0	θ_1
2	Telescope lift	0	$+\pi/2$	0	$\theta_2 + \pi/2$
3	Telescope extension	-1.557	$-\pi/2$	d_3	0
4	Fork tilt	$+0.550$	$-\pi/2$	0	$\theta_4 - \pi/2$
5	Yaw rotation	0	$+\pi/2$	-0.100	$\theta_5 + \pi/2$
6	Roll rotation	0	$-\pi/4$	$+0.225$	θ_6

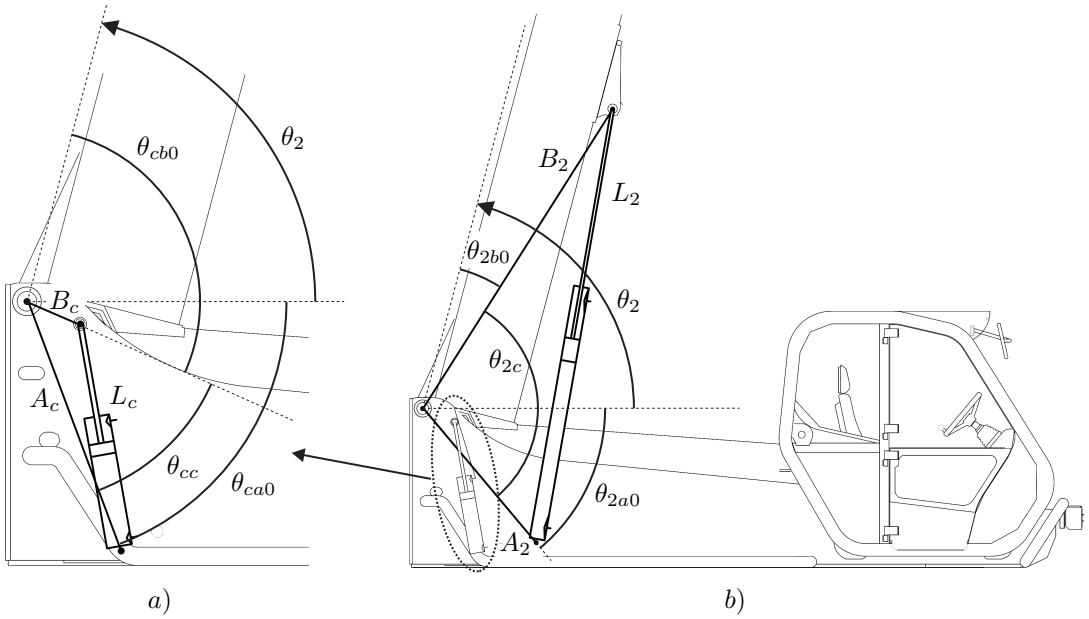

Figure 7: Nonlinear transformations between axis angular position and cylinder length for (a) compensation cylinder and (b) 2^{nd} axis

$$\begin{aligned} \theta_{4c} &= \theta_4 + \theta_{4a0} - \theta_{4b0} \\ L_4 &= \sqrt{A_4^2 + B_4^2 - 2A_4B_4cos(\theta_{4c})} \\ \dot{L_4} &= \frac{A_4B_4sin(\theta_{4c})}{L_4}\dot{\theta_4} \end{aligned} \tag{4}$$

$$\begin{aligned} \theta_{cc} &= \theta_2 + \theta_{ca0} - \theta_{cb0} \\ L_c &= \sqrt{A_c^2 + B_c^2 - 2A_cB_ccos(\theta_{cc})} \\ \dot{L_c} &= \frac{A_cB_csin(\theta_{cc})}{L_c}\dot{\theta_2} \end{aligned} \tag{5}$$

Cylinder velocities are used to obtain oil flow of the corresponding cylinder. Oil flow of the compensation cylinder passes through the fork tilt cylinder via the summing valve. Compensation cylinder extension causes fork tilt cylinder retraction, as is reflected in equation (6). Symbol ϕ_{v4} denotes oil flow of the fork tilt axis valve, ϕ_{c4} oil flow of the fork tilt axis cylinder and ϕ_{cc} oil flow of the compensation cylinder.

$$\phi_{c4} = \phi_{v4} - \phi_{cc} \tag{6}$$

4. Evaluation of closed-loop motion performance

4.1. Evaluation of motion performance in joint space

Motion performance of a single axis was assessed by analyzing trajectory tracking during point-to-point movement. Criteria included positional error and settling time to the final value while the response should be overdamped. Axis angle

Table 2: Resolution of axis angle (length) sensors

Axis number	Axis description	Sensor resolution
1	Turret rotation	0.008 $mrad$
2	Telescope lift	0.058 $mrad$
3	Telescope extension	0.04 mm
4	Fork tilt	0.058 $mrad$
5	Yaw rotation	0.058 $mrad$
6	Roll rotation	0.0006 $mrad$

(length) was measured with angular (length) sensors. The resolution of the sensors is given in Table 2. The evaluation was accomplished with the payload of 2000 kg and with diesel engine running at 1200 RPM.

4.2. Evaluation of motion performance in WCS

Straight line point-to-point movements were selected for evaluation of WCS mode of operation, since multi-axis motion was involved in this regime. Motion performance was assessed according to ISO 9283 standard (Manipulating industrial robots - Performance criteria and related test methods)[23]. Evaluation criteria included end-point repeatability, trajectory tracking and trajectory repeatability.

The end-point repeatability is defined as a radius of sphere containing all reached end-effector positions in n point-to-point movement repetitions. It is calculated according to equation (7). The coordinates of end-effector in reached position in repetition j are denoted as x_j, y_j and z_j. The mean values averaged over all repetitions are denoted as $\bar{x}$, $\bar{y}$ and $\bar{z}$. Distance of $j-th$ move end-position from the mean end-position is denoted as l_j. The size of a cluster of all end-positions is described by $\bar{l}$, and s states for standard deviation of $\bar{l}$. The repeatability r is calculated as a sum of cloud size $\bar{l}$ and 3 standard deviations s.

$$\begin{aligned} l_j &= \sqrt{(x_j-\bar{x})^2+(y_j-\bar{y})^2+(z_j-\bar{z})^2} \quad (7)\\ s &= \sqrt{\frac{\sum_{j=1}^{n}(l_j-\bar{l})^2}{n-1}} \\ \bar{l} &= \frac{1}{n}\sum_{j=1}^{n} l_j \\ r &= \bar{l}+3s \end{aligned}$$

The trajectory tracking error is defined as a maximum deviation of averaged measured positions from reference position along the whole path. In Fig. 9 the coordinates x_{ci}, y_{ci} and z_{ci} form $i-th$ point of the reference (commanded) path (T_{ci}). A normal plane to the reference path at point T_{ci} intersects the $j-th$ measured path at point T_{mij}: (x_{ij}, y_{ij}, z_{ij}). Mean coordinates of T_{mij} points for all n measured paths have coordinates $\bar{x_i}$, $\bar{y_i}$, $\bar{z_i}$ (point G_i). The distance AT_{pi} between point G_i and reference point T_{ci} is defined as trajectory tracking error at point T_{ci}. The total trajectory tracking error AT_p is maximum value of tracking error along whole reference path as noted in (8).

$$\begin{aligned} \bar{x_i} &= \frac{1}{n}\sum_{j=1}^{n} x_{ij},\ \bar{y_i} = \frac{1}{n}\sum_{j=1}^{n} y_{ij},\ \bar{z_i} = \frac{1}{n}\sum_{j=1}^{n} z_{ij} \quad (8)\\ AT_{pi} &= \sqrt{(\bar{x_i}-x_{ci})^2+(\bar{y_i}-y_{ci})^2+(\bar{z_i}-z_{ci})^2} \\ AT_p &= max[AT_{pi}],\ i=1\dots m \end{aligned}$$

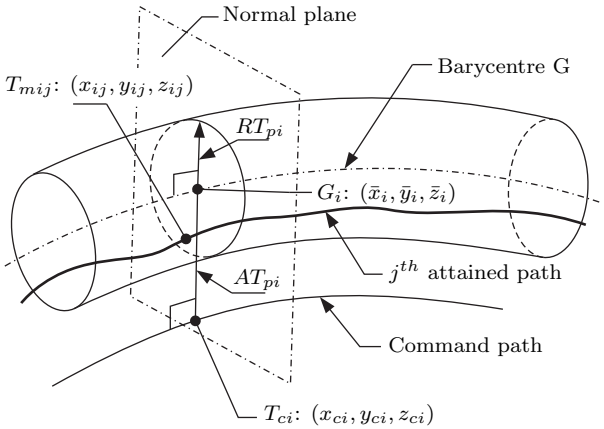

Figure 9: Evaluation of trajectory tracking according to ISO 9283 standard

The trajectory tracking repeatability RT_p is defined as maximum value of trajectory tracking repeatability of all m test points. Trajectory tracking repeatability at i-th point RT_{pi} is defined as a radius of circle containing all measured paths, as shown in Fig. 9. The repeatability RT_{pi} is calculated as a sum of radius of cluster containing all measured paths $\bar{l_i}$ and three standard deviations S_{li} according to (9).

$$\begin{aligned} l_{ij} &= \sqrt{(x_{ij}-\bar{x_i})^2+(y_{ij}-\bar{y_i})^2+(z_{ij}-\bar{z_i})^2} \quad (9)\\ \bar{l_i} &= \frac{1}{n}\sum_{j=1}^{n} l_{ij} \end{aligned}$$

$$
\begin{aligned}
S_{li} &= \sqrt{\frac{\sum_{j=1}^{n}(l_{ij}-\bar{l}_i)^2}{n-1}} \\
RT_{pi} &= \bar{l}_i + 3S_{li} \\
RT_p &= max[RT_{pi}],\ i = 1 \dots m
\end{aligned}
$$

The ISO 9283 standard defines ISO cube (see Fig. 10) for selection of points, lines and planes used for robot test movements. Test movements, employed for handler evaluation, are sketched in Fig. 10 by thick lines. The evaluation was accomplished with the payload of 2000 kg in 10 repetitions with diesel engine running at 1200 RPM.

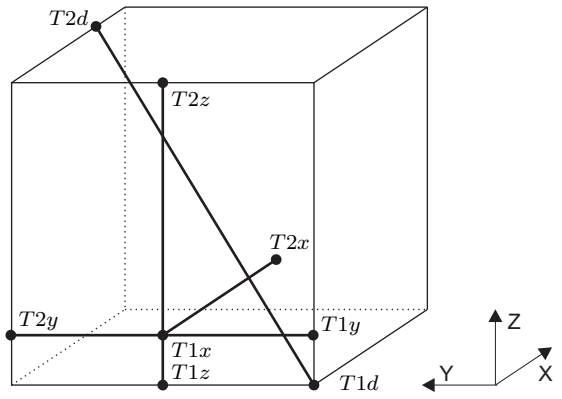

Figure 10: ISO cube for testing performance of robot manipulators as defined by ISO 9283 standard. For movements presented in section 5.2 the points connected by thick lines were used. Test point indices denote testing motion direction.

End-effector position was measured by an optical Optotrak Certus motion capture system. A set of line CCD cameras recorded 3D position of infrared markers attached to the end-effector with sub-millimeter accuracy ($\pm 0.15\ mm$ 1D error at distance of 2.25 m). Test movements were selected in a way that infrared markers were located inside the Optotrak measuring space. Test point coordinates are given in Table 3. Particular point indices denote the testing motion direction.

Usage of external, independent motion capture system instead of the joint sensors eliminated measurement errors due to inaccuracies in kinematic model. Inaccuracies include, for example, the effects of telescope bending due to loading, backlash due to clearance between telescope segments, and clearance in turret rotation reduction gear. Further source of errors was also inaccurate determination of kinematic parameters.

Table 3: Point coordinates and movement lengths, used for performance evaluation

Point	XYZ coordinates [m]	T1 to T2 distance [m]
T1x	[5.5 0.0 -0.5]	
T2x	[7.0 0.0 -0.5]	1.5
T1y	[5.5 -1.2 -0.5]	
T2y	[5.5 1.2 -0.5]	2.4
T1z	[5.5 0.0 -0.7]	
T2z	[5.5 0.0 0.5]	1.2
T1d	[6.6 1.0 0.5]	
T2d	[5.5 -1.2 -0.7]	2.737

5. Results

5.1. Single axis tracking

In Fig. 11 an example of closed-loop controlled response of the lift axis is presented. The reference position starts changing at time instant of 5.0 s with velocity following trapezoid profile. The handler respond with the delay of 0.8 s. The reference position reaches the final value at 13.7 s. The settling time to tolerance of 0.5 $mrad$, which is at telescope length of 10 m equivalent to 5 mm of end-effector displacement, is 1.3 s. The final position is reached asymptotically, without oscillations or overshoot.

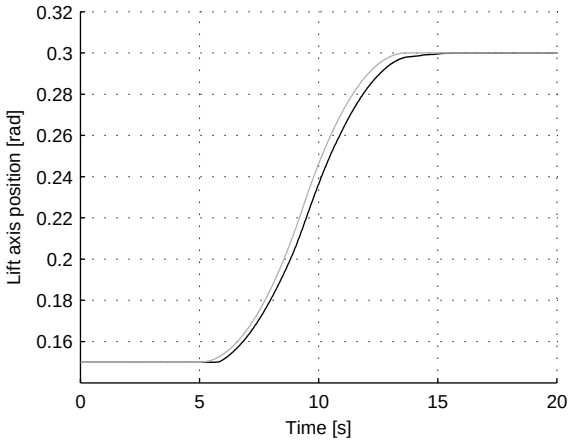

Figure 11: Closed-loop position control of the lift axis. Reference position (gray curve) and measured position (black curve) are shown.

5.2. WCS movement

Performance of WCS movement that involved multi-axis motion is presented by 4 examples of point-to-point movements, accomplished in forward

Table 4: Repeatability, trajectory tracking error and trajectory repeatability of WCS point-to-point movements

Movement	Repeatability r [mm]	Trajectory tracking error AT_p [mm]	Trajectory repeatability RT_p [mm]
T1x → T2x	1.3	46	6.2
T2x → T1x	1.1	47	4.5
T1y → T2y	5.4	59	51.3
T2y → T1y	7.0	63	32.0
T1z → T2z	2.7	32	9.0
T2z → T1z	1.5	16	7.9
T1d → T2d	3.9	53	39.9
T2d → T1d	4.2	59	22.4

and backward directions. Achieved end-point repeatability, trajectory tracking error and trajectory repeatability are shown in Table 4.

As an example, the tracking errors for 10 diagonal movement repetitions in both directions (T1d → T2d and T2d → T1d) are presented as a function of time in Fig. 12. The trajectory tracking errors AT_p for this example, determined according to (8), are shown in Fig. 13. The results show maximum tracking error of 59 mm for the T1d → T2d movement and 53 mm for the T2d → T1d movement.

Comparison of the trajectory tracking error calculated from Optotrak data (e.g. from independent reference measuring system) with the trajectory tracking error calculated from handler position sensors shows difference of up to 10 mm. The difference occurs due to mechanical imperfections of the handler, so it could be removed only by mechanical redesign of the telescope. Backlash in the telescope could be reduced by increasing stiffness of telescope segments and of joints between segments. This would reduce unmodeled kinematics and improve accuracy of the end-effector position calculated from handler's sensors.

Contribution of individual joint axes to common trajectory tracking error of the handler end-effector shows that the first axis (turret rotation) has largest contribution, followed by the second and third axis (telescope lift and extension). The control of telescope end-effector can be improved by improving control of individual axes, especially of the turret rotation axis. The turret rotation axis has significant backlash between the driving gear, attached to the hydraulic motor, and the driven internal gear wheel, attached to the turret, due to manufacturing of the internal gear wheel. The backlash has adverse effect on control performance by increasing hazard of control system induced oscillations, thus reducing acceptable controller gain.

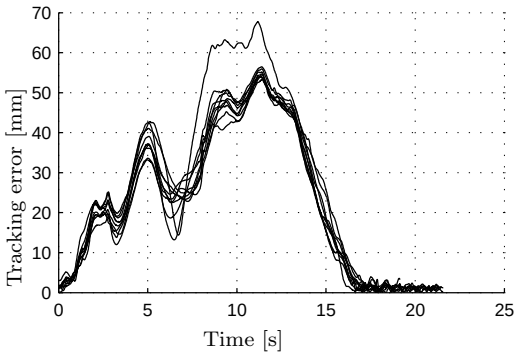

(a) Direction from T1d to T2d

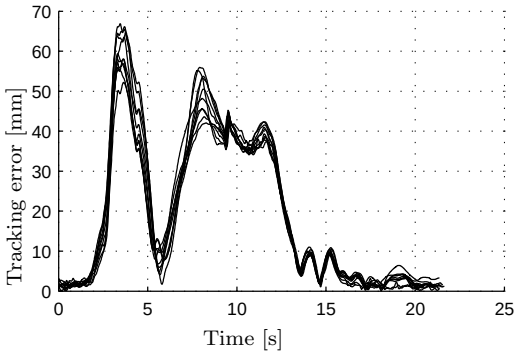

(b) Direction from T2d to T1d

Figure 12: Trajectory tracking errors, calculated for 10 repetitions of diagonal movement

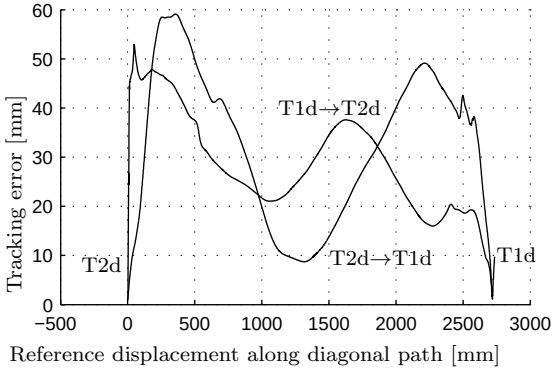

Figure 13: Trajectory tracking error of 10 point-to-point diagonal movements, calculated according to (8).

6. Discussion

During initial phase of development, an upgrade of a commercially available handler was chosen over a new design of the manipulator. Upgrade required addition of two hydraulic axes, position sensors, control computers and software.

New design from scratch was discussed as an option with handler producers at the moment of base handler selection. New design would require redesign of the handler's mechanics and actuation and control systems, what would also require to re-certificate the machine safety. The cost in such case would only be justified for a handler's producer if a series of at least ten machines would be sold per year. A redesign without strong cooperation with handler's producer would be more difficult and would open high risks.

During presented tests only constant payload of 2000 kg was used. To verify behavior of the handler with smaller load also tests with load 0 kg were performed. No significant difference was observed between both cases. This is explained by the significant mass of the telescope itself weighting about 2300 kg. It is reasonable to expect that the closed loop control will be stable with payloads in range from 0 to 2000 kg as it is stable with both extreme values.

Future works will be mainly focused on development of software for integration of the handler into semi-automated facade assembly system. The handler is driven manually during placement of the first panel and the facade position is recorded for later computer controlled operation. To ease operator's work, inclinometers are planned to be added to implement an automated levelling function and ultrasonic sensors will be used for measuring distance to the facade.

The developed robotic handler is applicable for other tasks involving lifting and carrying. Some proposed applications are structural beam placement, moving packs of cut timber at sawmill, waste handling and stacking of materials for recycling. Applicable would be every application that requires heavy load placement and larger workarea, movement in world coordinates, repeated or preprogrammed movements.

7. Conclusions

A closed-loop control system for a telescopic handler was developed. The closed-loop controlled handler is aimed to be used as a large scale manipulator in a semi-automated system for facade assembly.

The closed-loop control system is designed as an add-on to the original joystick driven control system. The handler original mechanics, hydraulics and controller were not altered. The handler mechanics was upgraded with two additional hydraulic axes to enable 6 DOFs motion of the handler end-effector. Position feedback sensors are implemented on all six axes. Existing safety algorithms, especially overturn prevention, are kept functional.

Additional computer control is implemented on two PC based computers. The GUI PC is used for interaction with handler operator, while core algorithms for handler motion control are executed by dedicated real-time RT controller. The developed closed-loop controller enables control of the end-effector motion along a straight line in Cartesian coordinate system either in a programmed or in a joystick directed motion mode. For safety assurance, a controller supervising module (WDT) was developed operating in addition to the safety mechanisms originally implemented in the handler.

Motion performance was verified by motion experiments. Handler end-effector position was measured by an optical 3D position tracking system, while results were evaluated according to ISO 9283 standard. Test results show that the worst case achieved repeatability of handler end-effector positioning is 7.0 mm. The worst case error of trajectory tracking is 63 mm, and the worst case achieved trajectory repeatability is 51 mm.

On the basis of measurement results, the functionality of the developed control system for closed-loop control of hydraulic telescopic handler has been proven. Measured accuracy of end-effector positioning in the range of few centimeters show that developed telescopic handler meets the requirements for facade panel assembly automation.

Acknowledgment

This work was financially supported by Trimo d.d., Slovenia, and by European Commission (EUREKA program, project E!-3902 - ETECH). Authors gratefully acknowledge contributions of Šantavec Miha, dipl. ing., and Zupančič Danijel, M.Sc., Trimo d.d., and Gračner Marko, dipl. ing., and Kovač Igor, D.Sc., Technische Universität Wien.

References

[1] W. C. Stone, NIST construction automation program, report No. 2, Proceedings of the NIST construction automation workshop, March 30-31, 1995, Gaithersburg, Maryland, 1996.

[2] A. M. Lytle, K. S. Saidi, W. C. Stone, J. L. Gross, Report of the NIST workshop on automated steel construction, in: W. C. Stone (Ed.), Proc. of the 19th International Symposium on Automation and Robotics in Construction (ISARC 2002), NIST, Gaithersburg, MD, 2002, pp. 247-254.

[3] Y. Hasegava, A new wave of construction automation and robotics in Japan, in: Proc. of the 17th International Symposium on Automation and Robotics in Construction (ISARC 2000), Taipei, Taiwan, 2000, pp. K15-K19.

[4] A. Stentz, Robotic technologies for outdoor industrial vehicles, in: G. R. Gerhart, C. M. Shoemaker (Eds.), Proceedings of SPIE AeroSense, Unmanned Ground Vehicle Technology, Society of Photo-Optical Instrumentation Engineers, Orlando, USA, 2001, pp. 192-199.

[5] H. Tanijiri, B. Ishiguro, T. Arai, R. Yoshitake, M. Kato, Y. Morishima, N. Takasaki, Development of automated weather-unaffected building construction system, Automation in Construction 6 (3) (1997) 215-227.

[6] F. van Gassel, The development of a concept for a Dutch construction system for high-rise buildings, in: F. Malaguti (Ed.), Proc. of the 22nd International Symposium on Automation and Robotics in Construction (ISARC 2005), Ferrara, Italy, 2005.

[7] D. Atsuhiro, H. Koji, K. Tomoya, S. Takashi, Development and application of automated delivery system for finishing building materials, in: W. C. Stone (Ed.), Proc. of the 19th International Symposium on Automation and Robotics in Construction (ISARC 2002), NIST, Gaithersburg, MD, 2002, pp. 235-240.

[8] K. Saidi, J. O'Brien, A. Lytle, Robotics in Construction, in: B. Siciliano, O. Khatib (Eds.), Springer Handbook of Robotics, Springer, Berlin, 2008, pp. 1079-1099.

[9] J.-Y. Park, P.-H. Chang, Vibration control of a telescopic handler using time delay control and commandless input shaping technique, Control Engineering Practice 12 (6) (2004) 769-780.

[10] D. Kim, J. Kim, K. Lee, C. Park, J. Song, D. Kang, Excavator tele-operation using a human arm, Automation in Construction 18 (2) (2009) 173-182.

[11] E. Budny, M. Chlosta, W. Gutkowski, Load-independent control of a hydraulic excavator, Automation in Construction 12 (3) (2003) 245-254.

[12] D. A. Bradley, D. W. Seward, The development, control and operation of an autonomous robotic excavator, Journal of Intelligent and Robotic Systems 21 (1) (1998) 7397.

[13] L. E. Bernold, Control schemes for tele-robotic pipe installation, Automation in Construction 16 (4) (2007) 518-524.

[14] E. Gambao, C. Balaguer, F. Gebhart, Robot assembly system for computer-integrated construction, Automation in Construction 9 (2) (2000) 479-487.

[15] P. Gonzales de Santos, J. Estremera, M. A. Jimenez, E. Garcia, M. Armanda, Manipulators help out with plaster panels in construction, Industrial robot: an international journal 30 (2) (2003) 508-514.

[16] P. Gonzales de Santos, J. Estremera, E. Garcia, M. Armanda, Power assist devices for installing plaster panels in construction, Automation in Construction 17 (4) (2008) 459-466.

[17] D. W. Seward, K. Zied, J. Riehl, A. Dolman, The development of a robotic system for tool deployment in hazardous environments, in: Proc. of the 17th International Symposium on Automation and Robotics in Construction (ISARC 2000), Taipei, Taiwan, 2000, pp. 179-184.

[18] E. Westkamper, R. D. Schaft, M. Schweizer, T. F. Herkommer, A. Meissner, Task-oriented programming of large redundant robot motion, Robotics and Computer-Integrated Manufacturing 14 (5/6) (1998) 363-375.

[19] T. A. Johansen, B. A. Foss, Constructing NARMAX models using ARMAX models, International journal of control 58 (5) (1993) 1125-1153.

[20] K. J. Hunt, T. A. Johansen, Design and analysis of gain-scheduled control using local controller networks, International journal of control 66 (5) (1997) 619-651.

[21] J. Denavit, R.S. Hartenberg, A kinematic notation for lower-pair mechanisms based on matrices, ASME Journal of Applied Mechanics 23 (1955) 215-221.

[22] L. Sciavicco and B. Siciliano, Modelling and Control of Robot Manipulators, Second Edition, Springer, Berlin, 2000.

[23] International standard ISO 9283:1998, Manipulating industrial robots - Performance criteria and related test methods, Second Edition, International Organization for Standardization, Geneve, Switzerland.